

# Extraction of $\gamma n \rightarrow \pi N$ observables from deuteron-target data

Satoshi X. Nakamura<sup>1</sup>

<sup>1</sup>*Laboratório de Física Teórica e Computacional - LFTC,  
Universidade Cruzeiro do Sul, São Paulo, SP 01506-000, Brazil*

An examination is conducted on a commonly used procedure for extracting (un)polarized  $\gamma n \rightarrow \pi^- p$  and  $\gamma n \rightarrow \pi^0 n$  observables from  $d(\gamma, \pi^-)pp$  and  $d(\gamma, \pi^0)pn$  data, using a model that consists of the impulse term and the final-state interaction (FSI) terms due to nucleon- and pion-exchange. Recent experimental and theoretical analyses used an extraction method that does not impose a cut on the final  $\pi N$  invariant mass  $W$ . I demonstrate that the use of this method can result in the  $\gamma n \rightarrow \pi N$  observables that are seriously distorted by the nucleon Fermi motion, and that one can efficiently avoid this problem by imposing a cut on  $W$ . It is also shown that the use of kinematical cuts of recent experimental analyses can still leave in the selected samples substantial FSI effects that must be corrected in extracting the  $\gamma n \rightarrow \pi N$  cross sections. In terms of the nucleon- and pion-exchange mechanisms, I give the first qualitative explanation of the FSI corrections, obtained in a recent MAMI experiment, for extracting  $\gamma n \rightarrow \pi^0 n$  cross sections.

Extracting (un)polarized cross sections for pion photoproduction off the neutron,  $\gamma n \rightarrow \pi^- p$  and  $\gamma n \rightarrow \pi^0 n$ , from the deuteron-target data,  $d(\gamma, \pi^-)pp$  and  $d(\gamma, \pi^0)pn$ , is an important task at photon facilities such as Jefferson Laboratory (JLab) [1–4] and MAMI [5–11], forming a base for studying the baryon spectroscopy. A commonly used procedure of extracting the  $\gamma n$  cross sections is to apply a certain set of kinematical cuts to the deuteron data and assume that the selected events are from single-nucleon quasi-free processes. For an accurate extraction, however, one may wonder what corrections are needed (or not) to account for final state interaction (FSI) effects remaining in the selected events. In the MAMI analysis [7, 11], the FSI corrections for  $\gamma n \rightarrow \pi^0 n$  cross sections were assumed to be the same as those for  $\gamma p \rightarrow \pi^0 p$ , which still needs a validation. Also, the validity of the applied cuts is a question. A theoretical analysis might answer these questions.

Tarasov et al. conducted a series of theoretical studies [1, 12, 13] on the FSI corrections needed to extract  $\gamma n$  cross sections. Their model for  $d(\gamma, \pi)NN$  is equipped with two-body  $\gamma N \rightarrow \pi N$ ,  $\pi N \rightarrow \pi N$  and  $NN \rightarrow NN$  elementary amplitudes generated with the SAID model [14], and the off-shell momentum dependence of the  $NN \rightarrow NN$  amplitudes (the other amplitudes) is assumed to be a monopole form [15] (constant at the on-shell values). They considered the impulse,  $N$ -exchange, and  $\pi$ -exchange mechanisms for  $d(\gamma, \pi^-)pp$  [1, 12], and estimated FSI corrections for extracting  $\gamma n \rightarrow \pi^- p$  cross sections. The FSI corrections were then used in JLab analyses [1, 4]. However, their extraction formula [Eq. (5) below] neglects a possible effect from the nucleon Fermi motion, which needs a validation. The authors also analyzed  $d(\gamma, \pi^0)pn$  [13] without including the  $\pi$ -exchange mechanism which was assumed to be negligible. Their predicted FSI corrections for  $\gamma N \rightarrow \pi^0 N$  cross sections turned out to be even qualitatively different from what has been found in the MAMI analysis [7, 11], which clearly calls for a further study.

In this Rapid Communication, I critically examine the extraction formula [Eq. (5) below] used in the JLab [1–4] and theoretical analyses [12, 13]. I point out that the neutron-target observables extracted with this formula can be seriously distorted by the Fermi motion. My calculation also finds significant FSI corrections, corresponding to kinematical cuts of the recent JLab analyses [1, 3, 4], needed to extract the neutron target observables. For the first time, I show that the FSI corrections, obtained in the MAMI analysis of  $d(\gamma, \pi^0)pn$  [7, 11], for  $\gamma N \rightarrow \pi^0 N$  cross sections are reasonably well explained by the  $N$ - and  $\pi$ -exchange FSI mechanisms; in particular, the  $\pi$ -exchange, which was ignored in Ref. [13], plays a crucial role. While no theoretical study has been done on FSI corrections for extracting  $\gamma n \rightarrow \pi N$  polarization observables of the current interests [3, 10], my analysis covers both unpolarized cross sections and polarization observables  $\Sigma$ ,  $E$ , and  $G$  [16].

The present analysis is based on a recently developed model for meson photoproduction off the deuteron [17, 18]. The model includes, for both  $d(\gamma, \pi^-)pp$  and  $d(\gamma, \pi^0)pn$ , the impulse,  $N$ -exchange, and  $\pi$ -exchange mechanisms as in previous investigations of  $d(\gamma, \pi)NN$  [19–22]. The ANL-Osaka model [23, 24] is used to generate the  $\gamma N \rightarrow \pi N$  and  $\pi N \rightarrow \pi N$  (off-shell) elementary amplitudes that are built in the deuteron reaction model. An update of  $\gamma n \rightarrow N^*$  ( $N^*$ : bare nucleon resonance) coupling parameters of the ANL-Osaka model has been made by including recent data for  $\gamma n \rightarrow \pi^- p$  [3, 4] and  $\gamma n \rightarrow \pi^0 n$  [7, 10] in the fit [17]. The initial deuteron wave function and half off-shell  $NN \rightarrow NN$  amplitudes are those from the CD-Bonn potential [25]. Comparisons of model predictions with data for  $d(\gamma, \pi)NN$  are presented in Ref. [17].

For extracting cross sections of  $\gamma n \rightarrow \pi N$  from those of  $d(\gamma, \pi)NN$ , a formula that gives a relation between them is necessary. For deriving it, one starts with the cross section formula for  $\gamma(\mathbf{q}) + d(\mathbf{p}_d) \rightarrow \pi(\mathbf{k}) + N_1(\mathbf{p}_1) + N_2(\mathbf{p}_2)$  [the laboratory-frame momenta are indicated in

the parentheses] as given by

$$d\sigma_{\gamma d} = (2\pi)^4 \delta^{(4)}(p_d + q - p_1 - p_2 - k) \left[ \frac{m_N}{E_{N_1}} \frac{m_N}{E_{N_2}} \frac{1}{2E_\pi} \right] \\ \times |M_{f,i}(E)|^2 \left[ \frac{1}{2E_d} \frac{1}{2E_\gamma} \right] d\mathbf{p}_1 d\mathbf{p}_2 d\mathbf{k}, \quad (1)$$

where  $E_x = \sqrt{\mathbf{p}_x^2 + m_x^2}$  is the energy for a particle  $x$  with the momentum  $\mathbf{p}_x$  and the mass  $m_x$ , and detailed formulas for the Lorentz invariant amplitude  $M_{f,i}(E = E_\gamma + m_d)$  are given in Ref. [17]. To isolate quasi-free events by removing contributions from the other nucleon and FSI, one conventionally applies a set of kinematical cuts to the data. Within my calculation, this amounts to restricting the phase-space integral in Eq. (1) to obtain  $d^2\sigma_{\gamma d}(E_\gamma)/dW d\cos\theta|_{\text{cut}}$  where, for  $N_2$  being treated as a spectator,  $W$  is the invariant mass of the final  $\pi$ - $N_1$  and  $\theta$  the angle between the momenta of  $\gamma$  and  $\pi$  in the  $\pi$ - $N_1$  center-of-mass (CM) frame. Then it is *assumed* that this partially integrated cross section is solely from the quasi-free processes integrated over the same phase-space. The resulting formula that can be used in analyzing data is

$$\left. \frac{d^2\sigma_{\gamma d}(E_\gamma)}{dW d\cos\theta} \right|_{\text{cut}} = \phi(W; E_\gamma) \frac{E'_\gamma}{E_\gamma} \frac{d\sigma_{\gamma n \rightarrow \pi N_1}(W)}{d\cos\theta}, \quad (2)$$

where  $E'_\gamma$  is defined by  $E'_\gamma = (W^2 - m_N^2)/(2m_N)$  and thus is the photon energy in the laboratory frame for  $\gamma n \rightarrow \pi N_1$ . The function  $\phi(W; E_\gamma)$  gives the probability of finding a process where the incident photon having  $E_\gamma$  hits a nucleon in the deuteron with an invariant mass  $W$ , and is determined by the nucleon momentum distribution in the deuteron  $\rho_d(p) \equiv u_s^2(p) + u_d^2(p)$  ( $u_{s,d}$ : the deuteron  $s, d$ -wave radial function) as:

$$\phi(W; E_\gamma) = \int d^3p_s \frac{m_N}{E_N(\mathbf{p}_s)} \delta(W - w(\mathbf{p}_s, E_\gamma)) \frac{\rho_d(|\mathbf{p}_s|)}{4\pi} \\ \times \prod_i \theta(x_i^{\text{max}} - x_i) \theta(x_i - x_i^{\text{min}}), \quad (3)$$

with

$$w(\mathbf{p}_s, E_\gamma) = \sqrt{(E_\gamma + m_d - E_N(\mathbf{p}_s))^2 - (\mathbf{q} - \mathbf{p}_s)^2}, \quad (4)$$

where  $\mathbf{p}_s$  is the spectator nucleon momentum;  $\{x_i\}$  are a set of kinematical variables and  $x_i^{\text{min}}$  ( $x_i^{\text{max}}$ ) is the minimum (maximum) value allowed by the cuts. Equations (2)-(4) agree with the formula presented in Ref. [12, 13, 26–28]. I also note that the relation between the  $\gamma d$  and  $\gamma n$  cross sections in Eqs. (2)-(4) becomes exact within my model when considering only the ‘quasi-free’ mechanism in which the incident photon interacts with only one of the nucleons inside the deuteron, ignoring the FSI terms, crossed terms, and the small deuteron  $d$ -state.

Equation (2) is the formula to extract the  $\gamma n \rightarrow \pi N_1$  cross section at a given  $W$  from  $d(\gamma, \pi)N_1 N_2$  data where the  $\pi N_1$  pair has the invariant mass  $W$ . This formula has been used in the MAMI analyses [5–11], but not in

TABLE I. Kinematical cuts A, B, and C. The cuts on the momenta for  $\pi^-$  ( $k_{\pi^-}$ ), faster proton ( $p_f$ ), slower proton ( $p_s$ ), and on the azimuthal angle difference between  $\pi^-$  and the faster proton ( $\Delta\phi = |\phi_{\pi^-} - \phi_{p_f}|$ ) in the 4-7th rows have been used in the references listed in the second row when extracting  $\gamma n \rightarrow \pi^- p$  observables (specified in the parentheses) from  $d(\gamma, \pi^-)pp$  data for the range of the photon energies listed in the third row.

	Cut A	Cut B	Cut C
Ref.	[1] ( $d\sigma/d\Omega$ )	[4] ( $d\sigma/d\Omega$ )	[3] ( $E$ )
$E_\gamma$ (MeV)	301 - 455	445 - 2510	700 - 2400
$k_{\pi^-}$ (MeV)	> 80	> 100	> 400
$p_f$ (MeV)	> 270	> 360	> 400
$p_s$ (MeV)	< 270	< 200	< 100
$ \Delta\phi - 180^\circ $	-	-	< 20°

recent JLab analyses [1, 3, 4]. The previous theoretical works [12, 13] presented a formula similar to Eq. (2), but did not use it either. The formula practically used in the JLab and theoretical analyses can be obtained by first assuming that  $d\sigma_{\gamma n \rightarrow \pi N_1}(W)/d\cos\theta$  in the r.h.s. of Eq. (2) is a constant in the range of  $W$  allowed by the kinematical cuts, and then integrating both sides of Eq. (2) over  $W$ . The resulting formula is

$$\left. \frac{d\sigma_{\gamma d}(E_\gamma)}{d\cos\theta} \right|_{\text{cut}} = \frac{d\sigma_{\gamma n \rightarrow \pi N_1}(\bar{W})}{d\cos\theta} \int d^3p_s \frac{m_N}{E_N(\mathbf{p}_s)} \frac{\rho_d(|\mathbf{p}_s|)}{4\pi} \\ \times \frac{E'_\gamma}{E_\gamma} \prod_i \theta(x_i^{\text{max}} - x_i) \theta(x_i - x_i^{\text{min}}), \quad (5)$$

and  $E'_\gamma/E_\gamma = E_N(\mathbf{p}_s)/m_N + \mathbf{p}_s \cdot \hat{\mathbf{q}}/m_N$ . The  $\gamma n \rightarrow \pi N_1$  cross sections extracted with this formula is an average over a certain range of  $W$  with a certain weight determined by  $E'_\gamma$ , the Fermi motion, and the cuts. The invariant mass  $\bar{W}$  for this averaged cross section is usually identified with the one for the incident photon and a nucleon at rest:  $\bar{W} = \sqrt{2m_N E_\gamma + m_N^2}$ . Equation (5) is thus based on the assumption that the average (smearing) due to the Fermi motion does not significantly invalidate this identification. I will critically examine the validity of this formula.

To proceed to a numerical study, the kinematical cuts need to be specified. I choose realistic ones, as summarized in Table I, from recent JLab analyses [1, 3, 4] where  $\gamma n \rightarrow \pi^- p$  observables were extracted from  $d(\gamma, \pi^-)pp$  data. In the previous theoretical studies [1, 12, 13], meanwhile, simpler cuts were used. For extracting the  $\gamma n \rightarrow \pi^0 n$  observable, I apply the same cuts to  $d(\gamma, \pi^0)pn$  by making obvious changes in the first column of Table I; ‘ $\pi^-$ ’  $\rightarrow$  ‘ $\pi^0$ ’, ‘Faster proton’  $\rightarrow$  ‘Neutron’, and ‘Slower proton’  $\rightarrow$  ‘Proton’. When extracting the  $\gamma n \rightarrow \pi N$  observables in this paper, I use Cut A (Cut B) for  $E_\gamma = 300$  (500) MeV. For  $E_\gamma > 700$  MeV, Cut B (Cut C) is used for extracting unpolarized differential cross sections (polarization asymmetries  $\Sigma$ ,  $E$ , and  $G$ ). I always

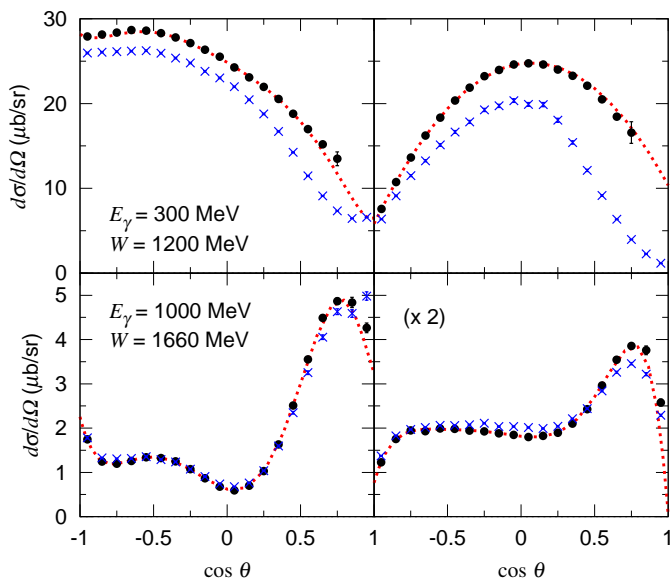


FIG. 1. Unpolarized differential cross sections for  $\gamma n \rightarrow \pi^- p$  (left) and  $\gamma n \rightarrow \pi^0 n$  (right) in the CM frame extracted from  $d(\gamma, \pi^-)pp$  and  $d(\gamma, \pi^0)pn$  data generated from my model including only the quasi-free mechanism;  $E_\gamma = 300$  (1000) MeV for the upper (lower) row. The black circles [blue crosses] are extracted using Eq. (2) [Eq. (5)], and  $W$  in Eq. (2) is indicated in the panels. The errors are only statistical from the Monte-Carlo integral, and are not shown when smaller than the point size. The red dotted curves are the free  $\gamma n \rightarrow \pi N$  cross sections at  $W$  from the ANL-Osaka model. The cross sections are scaled by the factor in the parenthesis when it is given.

take these choices for the cuts, unless otherwise stated.

To implement any kinematical cuts into the numerical computations, it is most convenient to use the Monte-Carlo method when performing the phase-space integrals in Eqs. (1), (3), and (5). The bin sizes (resolutions) for  $\cos\theta$  and  $W$  are taken to be 0.1 and 10 MeV, respectively, and thus a numerical value at  $x$  ( $= \cos\theta, W$ ) is understood to be the average over the range of  $x - \Delta/2 \leq x \leq x + \Delta/2$  where  $\Delta$  is the bin size. Therefore, all numerical results (except those for free  $\gamma n \rightarrow \pi N$  observables) are given with central values and their statistical errors associated with the Monte-Carlo method.

My investigation goes as follows. For a given choice of the kinematical cuts, my model generates  $d^2\sigma_{\gamma d}(E_\gamma)/dW d\cos\theta|_{\text{cut}}$  [ $d\sigma_{\gamma d}(E_\gamma)/d\cos\theta|_{\text{cut}}$ ] as ‘data’ from which  $d\sigma_{\gamma n \rightarrow \pi N}(W[\bar{W}])/d\cos\theta$  is extracted with Eq. (2) [Eq. (5)]. By comparing the extracted  $d\sigma_{\gamma n \rightarrow \pi N}(W[\bar{W}])/d\cos\theta$  with the corresponding one on a free neutron, which is calculated with the same elementary amplitudes used in calculating the  $\gamma-d$  cross sections, I can examine the extent to which the extracted cross sections are distorted by the FSI and/or the Fermi motion.

I first confirm in Fig. 1 [Fig. 2] that the extracted  $\gamma n \rightarrow \pi^0 n, \pi^- p$  unpolarized cross sections [ $E, G$ ] shown

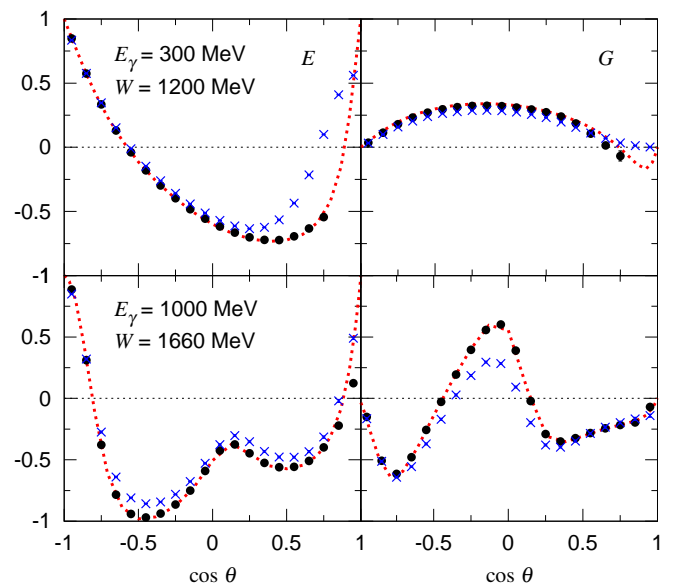


FIG. 2. The polarization observables  $E$  (left) and  $G$  (right) for  $\gamma n \rightarrow \pi^- p$  extracted from  $d(\gamma, \pi^-)pp$ . For  $E_\gamma = 300$  (1000) MeV, Cut A (Cut B) of Table I is used. The other features are the same as those in Fig. 1.

by the black circles reproduce the corresponding free ones given by the red dotted curves, when Eq. (2) is used for the extraction and the l.h.s. is calculated with the quasi-free mechanism only. The  $\gamma-n$  observables at  $W = \bar{W} = \sqrt{2m_N E_\gamma + m_N^2} \simeq 1200$  (1660) MeV are extracted from  $\gamma-d$  at  $E_\gamma = 300$  (1000) MeV. Cut A (Cut B) of Table I is used for  $E_\gamma = 300$  (1000) MeV. The absence of the black circles in the forward pion angles for  $E_\gamma = 300$  MeV is because these pion angles are not allowed by the kinematical cuts including the cut on  $W$ .

In the same figures, the blue crosses represent the  $\gamma n \rightarrow \pi^0 n, \pi^- p$  observables extracted with Eq. (5). Because Eq. (5) does not include the  $W$ -cut, the extracted  $\gamma-n$  observables are an average over a range of  $W \sim 1180-1210$  (1600-1700) MeV for  $E_\gamma = 300$  (1000) MeV. These  $\gamma-n$  observables are clearly different from the corresponding free ones in some cases. In particular, the extracted cross sections for  $\bar{W} = 1200$  MeV are significantly smaller than the free ones. This difference can be explained as follows. The  $\gamma n \rightarrow \pi N$  cross sections in the  $W = 1180-1210$  MeV region change rapidly and reach the  $\Delta(1232)$  peak near  $W \simeq 1200$  MeV. Because the blue crosses in Fig. 1 are the average of  $d\sigma_{\gamma n \rightarrow \pi N}(W)/d\cos\theta$  over this range of  $W$  (average of a  $W < 1200$  MeV region for  $\cos\theta \gtrsim 0.7$ ), they are necessarily smaller than the free ones at  $W = 1200$  MeV.

At  $E_\gamma = 1000$  MeV ( $\bar{W} = 1660$  MeV), on the other hand, the blue crosses in Fig. 1 reproduce the free cross sections fairly well in the  $\cos\theta < 0.5$  region. This is because the free cross sections in the range of  $W \simeq 1600-1700$  MeV has a mild and monotonic  $W$ -dependence, and

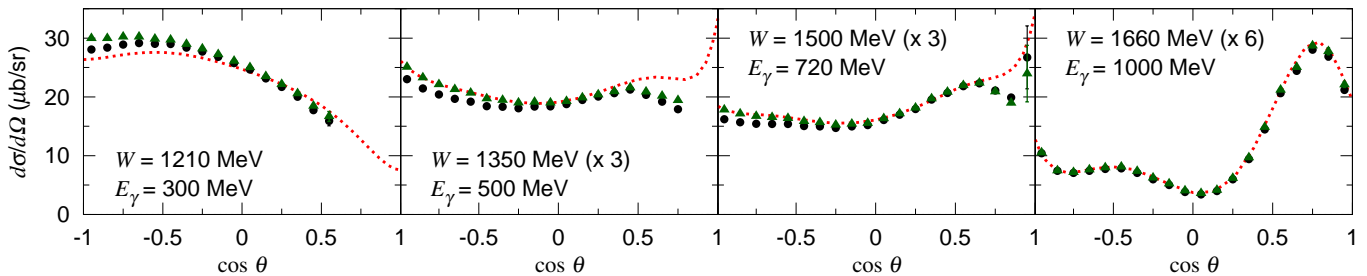


FIG. 3. The pion angular distribution for  $\gamma n \rightarrow \pi^- p$ . The black circles (green triangles) are extracted using Eq. (2) from  $d(\gamma, \pi^-)pp$  generated by my model including the impulse +  $N$ -exchange +  $\pi$ -exchange (impulse +  $N$ -exchange) terms. The other features are the same as those in Fig. 1.

hence the average is not significantly different from the free one at  $W = \bar{W}$ . In  $\cos \theta > 0.5$ , however, the average does not cancel out the  $W$ -dependence very well, giving the extracted cross sections visibly different from the free ones.

Differences between the blue crosses and red dotted curves are also seen in Fig. 2 for the polarization asymmetries of  $\gamma n \rightarrow \pi^- p$ , such as  $G$  at  $\bar{W} = 1660$  MeV. The difference again stems from averaging a rapid and non-monotonic  $W$ -dependence of  $G$  for the free  $\gamma n \rightarrow \pi^- p$  around  $W = 1660$  MeV. The asymmetry  $E$  at  $\bar{W} = 1200$  MeV also significantly deviates from the free one in  $\cos \theta \gtrsim 0.3$ . In these pion angles,  $\gamma n \rightarrow \pi^- p$  at  $W \sim 1200$  MeV in the deuteron are largely eliminated by the kinematical cuts, as implied by the absence of the black circles in  $\cos \theta \gtrsim 0.6$ , and  $\gamma n \rightarrow \pi^- p$  of  $W \sim 1120 - 1180$  MeV mainly contribute here. The average over this range of  $W$  gives the blue crosses which significantly deviate from the free  $E$  of  $W = 1200$  MeV. Thus Figs. 1 and 2 indicate that the neutron-target observables extracted with Eq. (5) can seriously suffer from the Fermi smearing, even when using the kinematical cuts of Table I where the cut on the spectator momentum ( $p_s$ ) should limit the  $W$ -range. One can avoid this problem by using Eq. (2) that includes the  $W$ -cut.

Now I study FSI effects on neutron-target observables extracted using Eq. (2). I calculate  $d(\gamma, \pi^-)pp$  cross sections including the impulse,  $N$ -exchange, and  $\pi$ -exchange (impulse and  $N$ -exchange) terms, apply the kinematical cuts, and extract  $\gamma n \rightarrow \pi^- p$  unpolarized differential cross sections as shown by the black circles (green triangles) in Fig. 3. The differences between these results and the free cross sections (red dotted curves) indicate that the extracted  $d\sigma_{\gamma n \rightarrow \pi^- p}(W)/d\Omega$  contain some FSI effects even after the kinematical cuts have been applied. At  $E_\gamma = 500$  and  $720$  MeV, the  $N$ -exchange ( $\pi$ -exchange) FSI effect is to visibly reduce the cross sections in the forward (backward) pion region, which is qualitatively consistent with the findings in Ref. [12]. Meanwhile, at  $E_\gamma = 1000$  MeV, a reduction due to the  $N$ -exchange in the forward pion angles is canceled by an enhancement due to the impulse crossed term.

The unpolarized  $\gamma n \rightarrow \pi^0 n$  differential cross sections extracted from  $d(\gamma, \pi^0)pn$  using Eq. (2) are shown in Fig. 4 (left). FSI effects are clearly larger than in the case of  $\gamma n \rightarrow \pi^- p$ . The  $N$ -exchange FSI largely reduce the cross sections at  $E_\gamma = 300$  MeV of the  $\Delta(1232)$  region. This is because the deuteron component (coherent process) is included in the  $NN$  plane wave from the impulse mechanism, and is eliminated by the scattering  $NN$   $^3S_1$  partial wave thanks to the orthogonality [19, 20]. Although the reduction due to the  $N$ -exchange FSI becomes smaller as the photon energy increases, it still persists in the forward pion region. Meanwhile, the  $\pi$ -exchange FSI effect is negligibly small at  $E_\gamma = 300$  MeV, as indicated by the small differences between the black circles and green triangles. As the photon energy increases, however, the  $\pi$ -exchange FSI significantly reduces the cross sections overall except the forward pion angles. On the other hand, in Ref. [13] where FSI corrections for extracting  $\gamma n \rightarrow \pi^0 n$  cross sections were theoretically estimated, the authors did not consider the  $\pi$ -exchange mechanism, assuming its effect negligible. As a result, the estimated FSI effects are only from the  $N$ -exchange mechanism and are visible only in the forward pion kinematics ( $\cos \theta \gtrsim 0.85$  for  $E_\gamma = 787$  MeV, for example).

The pronounced  $\pi$ -exchange FSI effect would call for an explanation because previous calculations [17, 19, 20, 22] showed it to be rather small for  $d(\gamma, \pi^0)pn$ . In the proton momentum distribution of  $d(\gamma, \pi^0)pn$  as shown in Fig. 5, the difference between the black solid and green dotted lines represents the  $\pi$ -exchange FSI effect. Without kinematical cuts, the  $\pi$ -exchange FSI reduces (enhances) the spectrum for  $p_p \lesssim 190$  ( $p_p \gtrsim 190$ ) MeV. The net  $\pi$ -exchange effect is small after integrating over  $p_p$ , and the previous calculations found this small effect. When the kinematical cuts are applied, the (spectator) proton momentum distribution becomes to the one shown in the insert. Because of cutting the large spectator momentum, the enhancement due to the  $\pi$ -exchange has been removed and only the reduction in the small spectator momentum region remains. This reduction appears as the significant  $\pi$ -exchange FSI effect in Fig. 4.

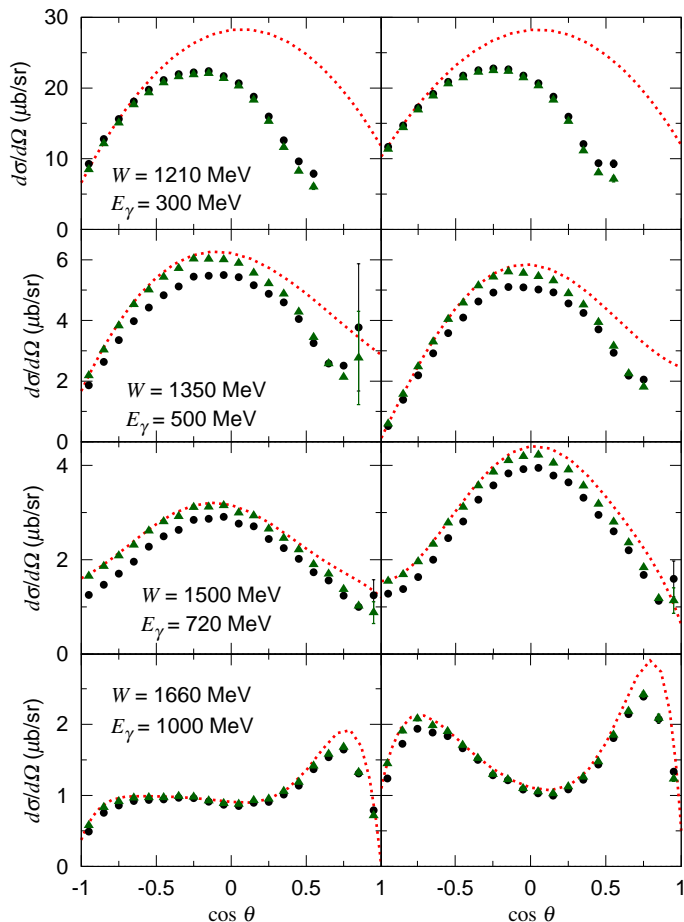


FIG. 4. (Left [Right]) The pion angular distribution for  $\gamma n \rightarrow \pi^0 n$  [ $\gamma p \rightarrow \pi^0 p$ ] extracted from  $d(\gamma, \pi^0)pn$ . The other features are the same as those in Fig. 3.

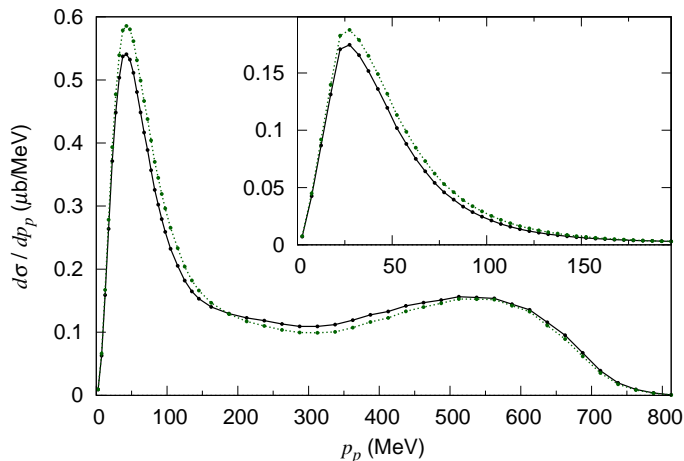


FIG. 5. Proton momentum ( $p_p$ ) distribution for  $d(\gamma, \pi^0)pn$  at  $E_\gamma = 500$  MeV. The points connected by the black solid (green dotted) lines are from my model including the impulse +  $N$ -exchange +  $\pi$ -exchange (impulse +  $N$ -exchange) terms. Insert: Same distribution but Cut B ( $p_s = p_p$ ,  $p_f = p_n$ ) and the  $W$ -cut ( $|W - 1350| < 5$  MeV) have been applied.

The  $\gamma p \rightarrow \pi^0 p$  cross sections have been also extracted from  $d(\gamma, \pi^0)pn$  and shown in Fig. 4 (right). Comparing with Fig. 4 (left), one can see that the FSI-induced reduction factors  $R_{\text{FSI}}$ , defined by the black circles divided by the red dotted curves (thus also including effects from the impulse crossed term), for  $\gamma n \rightarrow \pi^0 n$  and  $\gamma p \rightarrow \pi^0 p$  are within a few percents difference in most cases. This may partially support the assumption in the MAMI analysis [7, 11] that the FSI effects are the same for both. However, the FSI effects are sometimes more different. In the third row of Fig. 4 and  $\cos \theta \sim -1$ , for example,  $R_{\text{FSI}} \sim 0.74$  (0.81) for  $\gamma n \rightarrow \pi^0 n$  ( $\gamma p \rightarrow \pi^0 p$ ). The MAMI analysis [7, 11] obtained the experimental counterpart to  $R_{\text{FSI}}$ , denoted by  $R_{\text{FSI}}^{\text{exp}}$ , using their  $\gamma p \rightarrow \pi^0 p$  cross section data measured on hydrogen and deuterium targets. One can find that  $R_{\text{FSI}}$  for  $\gamma p \rightarrow \pi^0 p$  from my calculation is qualitatively very similar to  $R_{\text{FSI}}^{\text{exp}}$ . For a more quantitative comparison, the same kinematical cuts as in Refs. [7, 11] should be used because the FSI effects can depend on the choice of cuts. Still, my model explains a major fraction of  $R_{\text{FSI}}^{\text{exp}}$  for the first time.

It has been clearly shown that unpolarized differential cross sections for  $\gamma n \rightarrow \pi N$  extracted with Eq. (2) and the kinematical cuts listed in Table I need to be appropriately corrected for the FSI. It is however not trivial to develop a formula giving the necessary correction factors  $R_{\text{FSI}}^{-1}$ , since the corrections strongly depend on  $E_\gamma$ ,  $W$ ,  $\theta$  (pion angle), and cuts. The use of a dynamical model, such as used in this paper, to calculate the corrections for each data analysis is perhaps necessary in practice. A final remark is that the extracted polarization asymmetries  $\Sigma$ ,  $E$ , and  $G$  for  $\gamma n \rightarrow \pi N$  are numerically confirmed to be reasonably safe from distortions caused by the FSI, provided that the extraction is done with Eq. (2).

The author thanks H. Kamano, T.S.-H. Lee, and T. Sato for useful discussions. The author also thanks A. Sandorfi, T. Kageya, D. Carman, B. Krusche, and M. Dieterle for useful information on their experimental data and encouragements. This work is in part supported by Fundação de Amparo à Pesquisa do Estado de São Paulo (FAPESP), Process No. 2016/15618-8. Numerical computations in this work were carried out with SR16000 at YITP in Kyoto University, the High Performance Computing system at RCNP in Osaka University, the National Energy Research Scientific Computing Center, which is supported by the Office of Science of the U.S. Department of Energy under Contract No. DE-AC02-05CH11231, and the use of the Bebop [or Blues] cluster in the Laboratory Computing Resource Center at Argonne National Laboratory.

[1] W.J. Briscoe, A.E. Kudryavtsev, P. Pedroni, I.I. Strakovsky, V.E. Tarasov, and R.L. Workman, Phys.

- Rev. C **86**, 065207 (2012).
- [2] W. Chen, H. Gao, W.J. Briscoe, D. Dutta, A.E. Kudryavtsev, M. Mirazita, M.W. Paris, P. Rossi, S. Stepanyan, I.I. Strakovsky, V.E. Tarasov, and R.L. Workman, Phys. Rev. C **86**, 015206 (2012); W. Chen et al. (CLAS Collaboration), Phys. Rev. Lett. **103**, 012301 (2009).
- [3] D. Ho et al. (CLAS Collaboration), Phys. Rev. Lett. **118**, 242002 (2017).
- [4] P.T. Mattione et al. (CLAS Collaboration), Phys. Rev. C **96**, 035204 (2017).
- [5] K. Kossert et al., Eur. Phys. J. A **19**, 391 (2004).
- [6] D. Werthmüller et al. (A2 Collaboration), Phys. Rev. Lett. **111**, 232001 (2013).
- [7] M. Dieterle et al. (A2 Collaboration), Phys. Rev. Lett. **112**, 142001 (2014).
- [8] D. Werthmüller et al. (A2 Collaboration), Phys. Rev. C **90**, 015205 (2014).
- [9] L. Witthauer et al. (A2 Collaboration), Phys. Rev. C **95**, 055201 (2017).
- [10] M. Dieterle et al., Phys. Lett. **B770**, 523 (2017).
- [11] M. Dieterle et al. (A2 Collaboration), Phys. Rev. C **97**, 065205 (2018).
- [12] V.E. Tarasov, W.J. Briscoe, H. Gao, A.E. Kudryavtsev, and I.I. Strakovsky, Phys. Rev. C **84**, 035203 (2011).
- [13] V.E. Tarasov, W.J. Briscoe, M. Dieterle, B. Krusche, A.E. Kudryavtsev, M. Ostrick, and I.I. Strakovsky, Phys. Atom. Nucl. **79**, 216 (2016).
- [14] R.A. Arndt, W.J. Briscoe, I.I. Strakovsky, and R.L. Workman, Phys. Rev. C **66**, 055213 (2002); *ibid.* **76**, 025209 (2007); M. Dugger et al. (CLAS Collaboration), Phys. Rev. C **76**, 025211 (2007).
- [15] M.I. Levchuk, A.Yu. Loginov, A.A. Sidorov, V.N. Stibunov and M. Schumacher, Phys. Rev. C **74**, 014004 (2006).
- [16] A.M. Sandorfi, S. Hoblit, H. Kamano, and T.-S.H. Lee, J. Phys. G **38**, 053001 (2011).
- [17] S.X. Nakamura, H. Kamano, T.-S.H. Lee, and T. Sato, arXiv:1804.04757 [nucl-th].
- [18] S.X. Nakamura, H. Kamano, and T. Ishikawa, Phys. Rev. C **96**, 042201(R) (2017).
- [19] E.M. Darwish, H. Arenhövel and M. Schwamb, Eur. Phys. J. **A16**, 111 (2003).
- [20] A. Fix and H. Arenhövel, Phys. Rev. C **72**, 064005 (2005).
- [21] M. Schwamb, Phys. Rep. **485**, 109 (2010).
- [22] J.-J. Wu, T. Sato, and T.-S.H. Lee, Phys. Rev. C **91**, 035203 (2015).
- [23] H. Kamano, S.X. Nakamura, T.-S.H. Lee, and T. Sato, Phys. Rev. C **88**, 035209 (2013).
- [24] H. Kamano, S.X. Nakamura, T.-S.H. Lee, and T. Sato, Phys. Rev. C **94**, 015201 (2016).
- [25] R. Machleidt, Phys. Rev. C **63**, 024001 (2001).
- [26] I. Blomqvist and J.M. Laget, Nucl. Phys. **A280**, 405 (1977).
- [27] J.M. Laget, Nucl. Phys. **A296**, 388 (1978).
- [28] J.M. Laget, Phys. Rep. **69**, 1 (1981).